Comparative Medicine
Copyright 2013
by the American Association for Laboratory Animal Science

Vol 63, No 3
June 2013
Pages 227–232

Original Research

Mouse Model of Muscle Crush Injury of the Legs

Georgina L Dobek,[1,*] Nadia D Fulkerson,[1] Jennifer Nicholas,[1] and Barbara St Pierre Schneider[1]

Because crush injury to skeletal muscle is an important cause of morbidity in natural disaster and battlefield settings, a reproducible and refined animal model of muscle crush injury is needed. Both open and closed small-animal models of skeletal muscle crush injury are available but are limited by their need for surgical isolation of the muscle or by the adverse effect of fibular fracture, respectively. In the current study, we developed and validated a novel, noninvasive mouse model of lower-extremity muscle crush injury. Despite the closed nature of our model, gross evidence of muscle damage was evident in all mice and was verified microscopically through hematoxylin and eosin staining. The injury elicited both neutrophil and macrophage infiltration at 24 and 48 h after injury. The area percentage and mean antigen area of F4/80-positive macrophages were higher at 48 h than at 24 h after injury, and CD68-positive macrophage area percentage and mean antigen area differed significantly between injured and uninjured muscle. In addition, the incidence of fibular fracture was one third lower than that reported for an alternative noninvasive model. In conclusion, our model is a reproducible method for muscle crush injury in the mouse pelvic limb and is a refinement of previous models because of its decreased bone fractures and reduction of animal numbers.

Abbreviation: AOI, area of interest.

Skeletal muscle crush injury is an important cause of morbidity in both civilian and military populations. During earthquakes, tornados, and other natural disasters, collapsed structures result in crush injuries in approximately 40% of victims entrapped in the rubble,[14] and crush injuries sustained during these events primarily affect skeletal muscle tissue.[13] Crush injuries to skeletal muscle received during military conflict can occur when a limb is compressed for an extended time period, and combat-related crush injuries of the extremities frequently are present in wounded troops who are transported via aeromedical evacuation.[22]

A muscle-crush injury is induced when pressure is applied to skeletal muscle, interrupting blood flow and damaging the cell membranes of the muscle fibers. Several animal models of skeletal muscle-crush injury are used to study the pathophysiology of acute muscle inflammation and to investigate potential therapies.[1,2,3,5,8,9,12,17,18,21] The most common model is the application of force to a surgically isolated pelvic limb muscle by using a clamp.[16] Although closed models have been investigated, these studies typically involve dropping weights onto rodents' pelvic limbs, thereby increasing the adverse event of fractures. Although not often reported in the literature, the incidence of fibular fractures in rats as a result of the dropped weight was 27% in one study.[3] An additional drawback to the dropped-weight model is that it simulates a high-force contusion injury and does not provide the ischemic effect of the continuous pressure applied by the open clamp model. The ideal crush-injury model would mimic a force-induced injury, because 40% of survivors trapped in building rubble develop ischemia-induced crush syndrome.[14]

Received: 27 Jul 2012. Revision requested: 04 Sep 2012. Accepted: 09 Dec 2012.
[1]School of Nursing, University of Nevada, Las Vegas, Las Vegas, Nevada.
[*]Corresponding author. Email: georgina.dobek@unlv.edu

We chose to investigate a novel model of closed crush injury for several reasons. An animal model of skeletal muscle injury should mimic the human clinical presentation, and a closed model more closely simulates a real-world crush injury. Second, because the incision created in the open model can activate the inflammatory response, a group of sham-operated animals is needed to control for the variable of the incision-induced inflammation. By using a closed model, the contralateral limb can serve as the uninjured control, thereby reducing the number of animals needed to perform the study. Last, the closed model represents a refinement of the crush injury procedure by removing the additional tissue damage and inflammation that result from the incision and tissue dissection of the surgical procedure and by reducing the incidence of fractures.

Because this model has not been described in the literature, the objective of the current study was to develop a closed, sustained-force model of lower-extremity crush injury that induces a measurable leukocyte response and minimizes damage to nearby bones. In addition, we used monoclonal antibodies to characterize the leukocyte populations associated with this skeletal muscle crush injury model.

Materials and Methods

Animals. Male C57BL/6NHsd mice (*Mus musculus*; $n = 10$; age, 6 to 7 wk) were purchased from Harlan Laboratories (Indianapolis, IN) and allowed at least 5 d to acclimate before the start of the study. All mice were vendor-verified prior to shipping to be free of ectoparasites, helminth endoparasites, and antibodies to 19 murine viruses. Animals were housed in an AAALAC-accredited facility at the University of Nevada (Las Vegas, NV). Mice were individually housed under a 12:12-h light:dark cycle in static polycarbonate microisolation cages (Alternative Design, Siloam

Springs, AR) on 1/4-in. corncob bedding (Bed-O'Cobs, The Andersons, Maumee, OH). Cotton nesting material (Nestlets, Ancare, Bellmore, NY) was provided for enrichment. Tap water and rodent chow (Lab Diet 5001, PMI, St Louis, MO) were available ad libitum. All animal procedures were reviewed and approved by the University of Nevada, Las Vegas IACUC and were conducted in compliance with the recommendations in the *Guide for the Care and Use of Laboratory Animals*.[7]

Muscle injury. The mice were randomly assigned to either a 24- or 48-h postinjury group. The force delivered by the crush injury device was calibrated between mice. Mice were weighed and then given buprenorphine (0.05 to 0.1 mg/kg SC; Buprenex, Reckitt Benckiser Pharmaceuticals, Richmond, VA). At 20 min after buprenorphine administration, the mouse was anesthetized with isoflurane via nose cone. The mouse was placed on the crush injury device platform in dorsal or sternal recumbancy to create a crush injury on the medial or lateral surface of the gastrocnemius muscle, respectively (Figure 1). The right pelvic limb was secured with tape, and the crush injury piston was situated directly over the area to be injured, in direct contact with the skin. An air compressor (model D55140, Dewalt, Baltimore, MD) delivered pressure at 45 psi to the piston for 30 s, providing a force of 28.5 to 30.4 N, at 1 to 3 locations overlying the gastrocnemius muscle. The contralateral pelvic limb served as the uninjured control. After the crush injury was generated, mice were allowed to recover in the animal housing facility for 24 or 48 h. Additional doses of buprenorphine were administered every 12 h after the first dose until the time of euthanasia. In addition, mice were assessed twice daily by a veterinarian (GLD) for signs of unrelieved pain such as piloerection of fur, reluctance to ambulate, overgrooming of the injured limb, and abnormal gait or posture.

After the recovery period, mice were anesthetized with isoflurane, and the plantar flexor muscles (gastrocnemius, soleus, and plantaris) were collected and frozen for leukocyte analysis in melting isopentane (Fisher Scientific, Pittsburgh, PA) cooled by liquid nitrogen. All frozen muscles for leukocyte analysis were stored at –70 °C. After tissue collection, mice were euthanized under anesthesia by cervical dislocation, and the fibula and tibia were dissected to assess the presence of fractures.

Preparation of muscle cross-sections. Serial cross-sections (thickness, 10 µm) at the sites of the hematomas were obtained by using a cryostat (model CM1850, Leica Microsystems, Bannockburn, IL). Cross-sections were applied to poly-L-lysine-coated slides and stored at –70 °C until immunolabeling. Muscle sections were stained with hematoxylin and eosin for histologic assessment of fiber damage and cell infiltration.

Immunolabeling. Leukocytes were immunolabeled by using 5 primary monoclonal antibodies: rat antimouse Ly6G (clone 1A8, BD Biosciences Pharmingen, San Diego, CA); rat antimouse 7/4 (AbD Serotec, Raleigh, NC); rat antimouse Ly6C/G (Gr1, Invitrogen, Carlsbad, CA); rat antimouse CD68 (AbD Serotec); and antimouse F4/80 (Invitrogen). These antibodies detect neutrophils and granulocytes (Gr1 and 1A8),[6] neutrophils and monocytes (7/4),[15] and macrophages (CD68 and F4/80).[4,10]

Muscle sections were air-dried and then fixed in room temperature acetone. After a rinse in PBS, nonspecific binding was blocked by using 2% bovine serum albumin in PBS. The slides were rinsed in PBS, and then the primary antibody (7/4, anti-Ly-6G, anti-Ly-6C/G, and F4/80, 1:20 dilution; anti-CD68, 1:100 dilution) was applied to individual sections for 2 h. Sections were rinsed again in PBS and then the secondary antibody, biotinylated antirat IgG (mouse adsorbed, 1:200; Vector Laboratories, Burlingame, CA), was applied for 30 min followed by a PBS rinse. Endogenous peroxidase was quenched with 0.3% hydrogen peroxide in methanol. After a PBS rinse, the sections were incubated with Vectastain ABC peroxidase reagent (Vector Laboratories) for 30 min and then rinsed again with PBS. Vector VIP substrate solution (Vector VIP Substrate Kit, Vector Laboratories) was applied for 1 min (for sections incubated with 7/4 antibody) or 3 min (for other antibodies), followed by a rinse in double-distilled water to stop the substrate reaction. The sections were dehydrated with 95% and 100% ethanol and cleared twice with Hemo De (Scientific Safety Solvents, Keller, TX), and coverslips were mounted by using a nonaqueous medium (Cytoseal 60, Fisher Scientific). Control sections were generated as described, except a 2-h incubation with PBS was substituted for the primary antibody step. After the sections were coverslipped, each slide was coded to cover any identifying information marked on the slide.

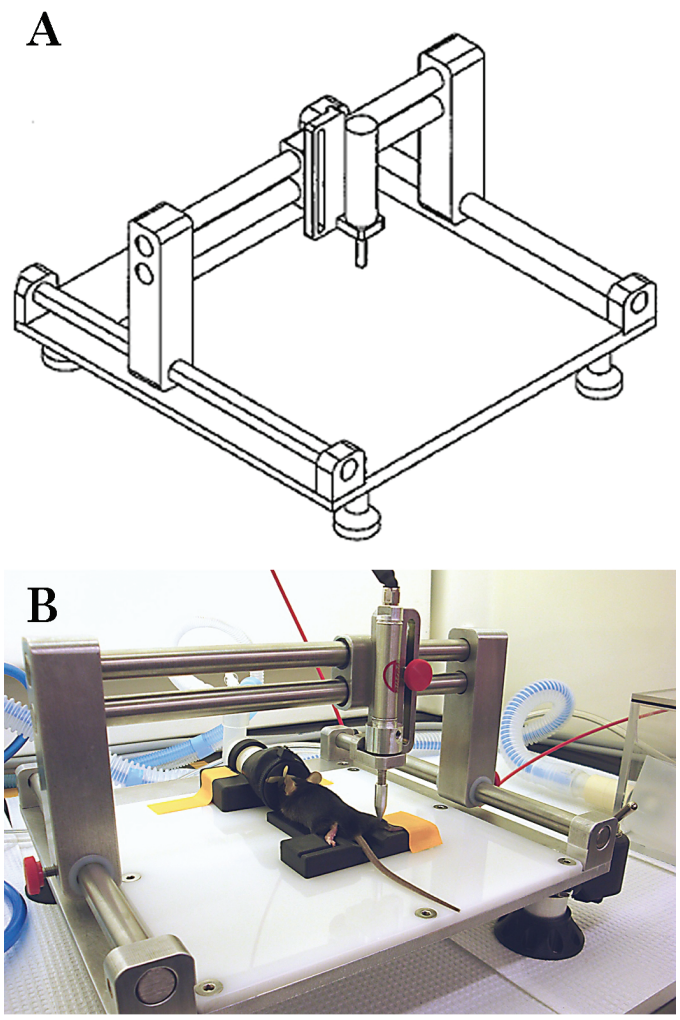

Figure 1. (A) Line drawing of the crush-injury device and (B) a photograph of a mouse on top of a plastic trough (for restraint), with the outstretched right pelvic limb situated underneath the injury delivery piston.

Image analysis. For all assessed antibodies, a computer-assisted approach was used to quantify immunolabeling. For each section,

24-bit images (red, green, and blue) were captured by using a light microscope (Eclipse E600, Nikon, Melville, NY), 10× objective (magnification, 100×), a color mosaic camera (SPOT RT KE, Diagnostics Instruments, Sterling Heights, MI), and Image-Pro Plus 5.1.2 software (Media Cybernetics, Silver Spring, MD) on a computer (Optiplex GX280 with 1905FP monitor, Dell, Round Rock, TX).

CD68 antibody. Images of CD68-immunolabeled sections from injured and uninjured limbs were captured from an area of interest (AOI, 1.00 mm^2) with the most staining within the lateral gastrocnemius muscle. An image of the same area was generated from a PBS-treated control slide and, to facilitate matching the antibody- and PBS-treated AOI, each PBS section was no more than 4 sections away from the immunolabeled section. Due to the presence of resident CD68-positive macrophages in uninjured muscle, a larger AOI was used for this antibody to ensure that these macrophages were included in the analysis of the injured and uninjured muscle sections. Once the images were captured, a second observer checked the AOI to confirm that both slides were from the same anatomic area and to examine the PBS section for false-positive immunolabeling or debris. Muscle features such as connective tissue greater than 14 µm in width, blood vessels, nerve bundles, and muscle spindles in the antibody-treated AOI were 'erased' manually so that these objects were not included in the measured area. Debris observed in the PBS AOI was manually erased from the antibody AOI. This erasing was double-checked by a second observer.

After converting the images to 8-bit gray scale, the lowest and highest pixel limits were defined. The threshold value was determined by assigning pixels to objects within the AOI based on 3 immunolabeled cells of medium intensity as viewed on the computer screen. A second observer confirmed that the 3 cells were of medium intensity and independently selected a threshold value according to the marked cells. When the 2 threshold values differed by 1, then the highest threshold value was used. When the values differed by 2, then the middle value was chosen. When the threshold values were not within 15% of each other or when they differed by more than 2, then the observers discussed the discrepancy to decide on the final threshold value. The data points (sum, samples, min, max, range, mean, and standard deviation) acquired from the final threshold value were exported to Excel 2010 (Microsoft, Redmond, WA). For each adjusted AOI, number of positive cells, area percentage, and mean antigen area were determined. The positive cell number is identified by the Image-Pro Plus 5.1.2 software as the number of samples. The percentage of area of antigen immunolabeling (area percentage) was calculated by converting the pixels to area ($µm^2$), dividing this value by the adjusted AOI area, and then multiplying the quotient by 100%. The mean antigen area is the mean size of the antibody-positive objects. This value was generated by the Image-Pro Plus 5.1.2 software by dividing the stained area of the AOI by the total number of cells present. Means and SE were calculated for each variable for the injured and uninjured groups.

F4/80, 1A8, 7/4, and Gr1 antibodies. Sections labeled with F4/80, 1A8, 7/4, and Gr1 antibodies were analyzed similarly to the CD68 sections, except that the AOI was decreased to 0.067 mm^2 and generated from the area with the most staining within the lateral gastrocnemius muscle. Blood vessels, connective tissue spacing, and nerve bundles were avoided during AOI placement, and debris was erased from the images. Thresholds were defined by assigning pixels based on the overall staining pattern observed on the computer screen while not assigning pixels to extraneous muscle features. A second observer independently assigned a threshold, and differences in threshold values were resolved by using the same method as described earlier.

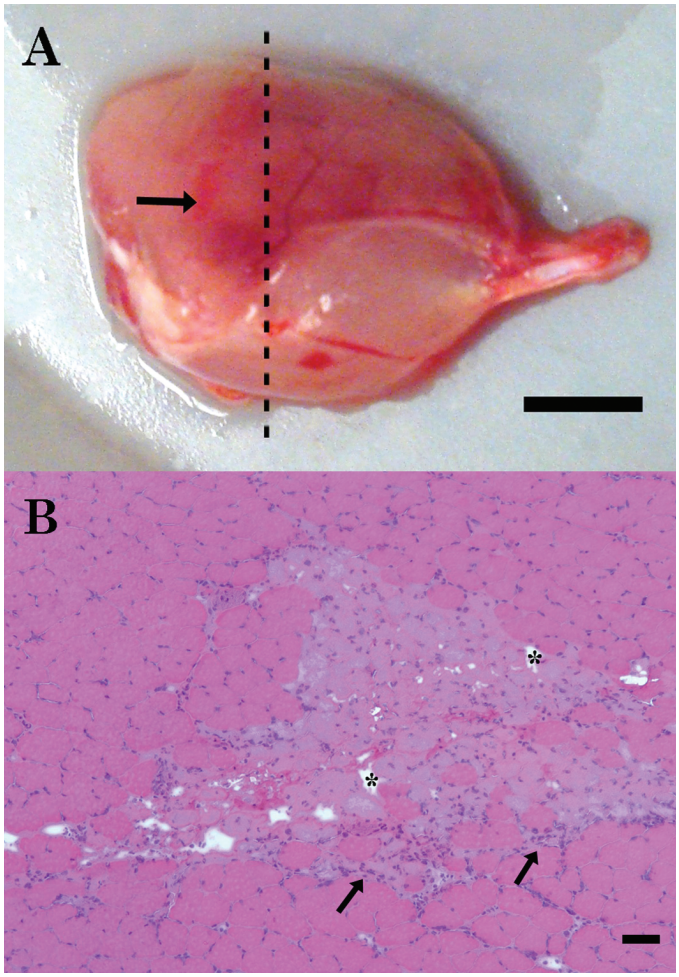

Figure 2. Representative images of the gross and histologic findings in the crush-injured lateral gastrocnemius muscle. (A) At 48 h after injury, there is a large, dark red hematoma (arrow) surrounded by pink, unaffected tissue. The dashed line indicates the location of the cross-section; bar, 2.5 mm. (B) Muscle fibers with multiple areas of necrosis are characterized by pale sarcoplasm, altered fiber shape, edema-induced spacing between fibers (asterisks), and leukocyte infiltration (arrows) and are surrounded by unaffected muscle tissue. Hematoxylin and eosin stain; bar, 50 µm.

Statistical analysis. Data were analyzed by using SAS version 9.2 (SAS Institute, Cary, NC) or SPSS versions 16 and 19 (IBM, Armonk, NY). For each antibody, the Wilcoxon rank-sum test (2-sided) was used to investigate any differences between the 2 time points (24 and 48 h) for 3 variables: area percentage; number; and mean antigen area. A one-sided Wilcoxon signed-rank test was used to examine the relationship between injured and uninjured muscles. A P value of less than 0.05 was considered statistically significant for all analyses.

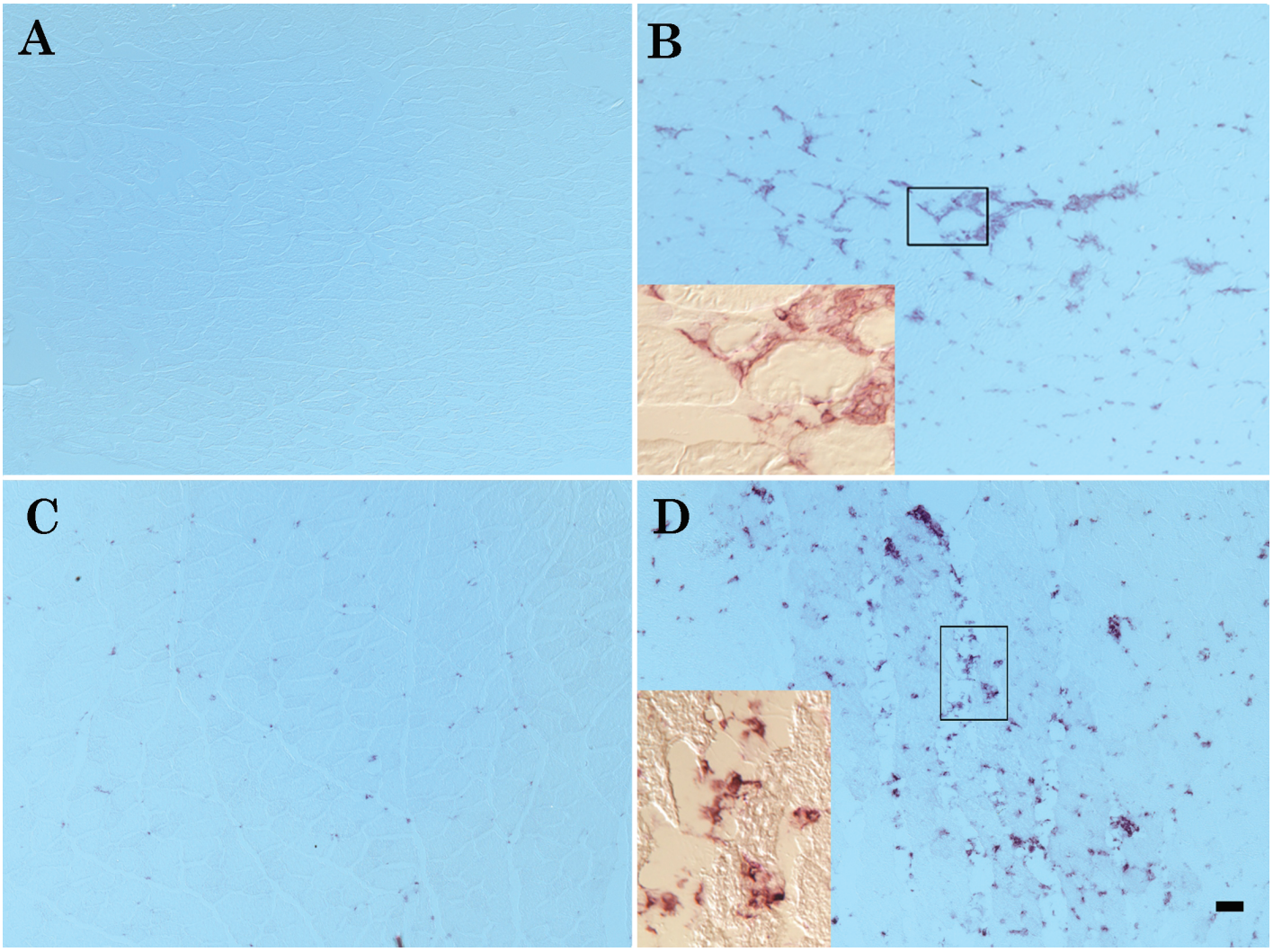

Figure 3. F4/80 and CD68 immunolabeling. (A) Uninjured lateral gastrocnemius muscle is negative for F4/80 staining. (B) Extensive invasion of lateral gastrocnemius muscle by F4/80-positive cells at 48 h after injury. (C) CD68-positive macrophages are present in the uninjured lateral gastrocnemius muscle. (D) CD68-positive macrophages increase in area percentage and size in the injured lateral gastrocnemius muscle at 48 h after injury. Bar, 50 µm. Insets at higher magnification (20×) show the positive cells surrounding and infiltrating the injured fibers.

Results

Mouse behavior. During the postinjury recovery period, all mice exhibited normal gait and posture and applied weight to all 4 limbs. Signs of unrelieved pain, such as piloerection of fur, hunched posture, reluctance to move, and over-grooming of the injured limb, were not observed.

Gross and histopathologic findings. At both the 24- and 48-h time points, a hematoma was spread diffusely in the lateral gastrocnemius muscle (Figure 2 A), and mild edema of the lower pelvic limb was noted. No femoral or tibial fractures were observed in any of the mice; 1 of the 10 (10%) mice had a fibular fracture.

Muscle damage was verified microscopically by using cross-sections of the lateral gastrocnemius muscle that were stained with hematoxylin and eosin (Figure 2 B). All mice had visible damage in the lateral gastrocnemius muscle of the injured pelvic limb. At both time points, injured lateral gastrocnemius muscle demonstrated pale sarcoplasm, edema-induced spacing between fibers, and leukocyte infiltration.

Leukocyte immunolabeling. No false-positive immunolabeling was observed in any PBS-treated section. Two time points, 24 and 48 h after injury, were examined for leukocyte analysis. Uninjured muscle was negative for Gr1, 1A8, 7/4, and F4/80 immunolabeling and had a few CD68-positive macrophages present. At both time points, neutrophils and macrophages had infiltrated injured muscle (Figure 3).

Three variables were analyzed for immunolabeling in the muscle AOI: area percentage of positive cells; number of positive cells; and mean antigen area. At 24 and 48 h after injury, CD68 area percentage and mean CD68 antigen area differed significantly (one-sided $P < 0.05$ for both comparisons) between injured and uninjured muscle (Figure 4). The number of CD68-positive cells did not change from 24 to 48 h (data not shown), but mean CD68 antigen area increased significantly ($P < 0.05$) from 24 to 48 h after injury. From 24 to 48 h after injury, there was a 4-fold increase ($P = 0.015$) in F4/80 area percentage and a significant ($P = 0.009$) increase in mean F4/80 antigen area (Figure 5), but the number

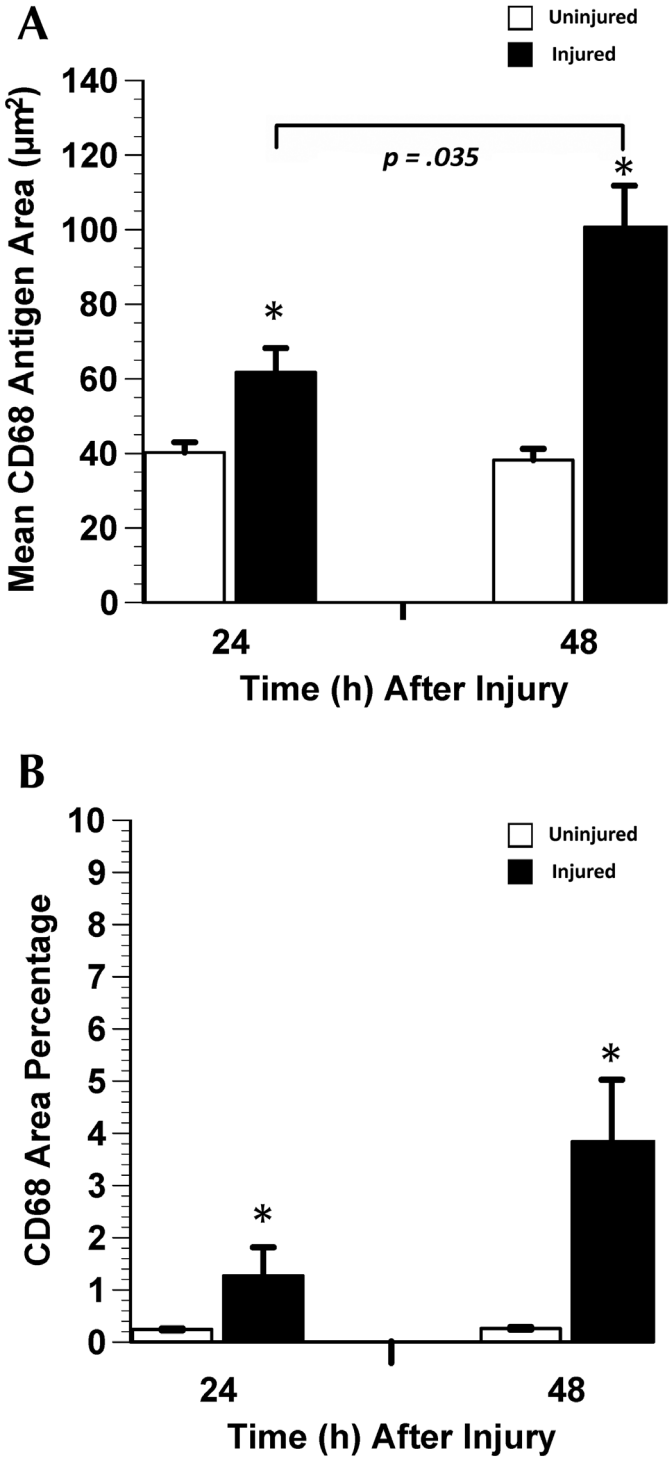

Figure 4. CD68-positive macrophage response to gastrocnemius muscle crush injury (mean ± SE). (A) CD68 antigen area is an indicator of cell size. Positive cells are significantly (*, $P < 0.05$) larger in injured than in uninjured lateral gastrocnemius muscle and at 48 h compared with 24 h. (B) There is a significant difference in CD68 area percentage between injured and uninjured muscles.

of F4/80-positive cells did not differ between the 2 time points (data not shown). Mean 1A8 antigen area decreased significantly ($P = 0.030$) by 43% from 24 to 48 h after injury (Figure 5 A),

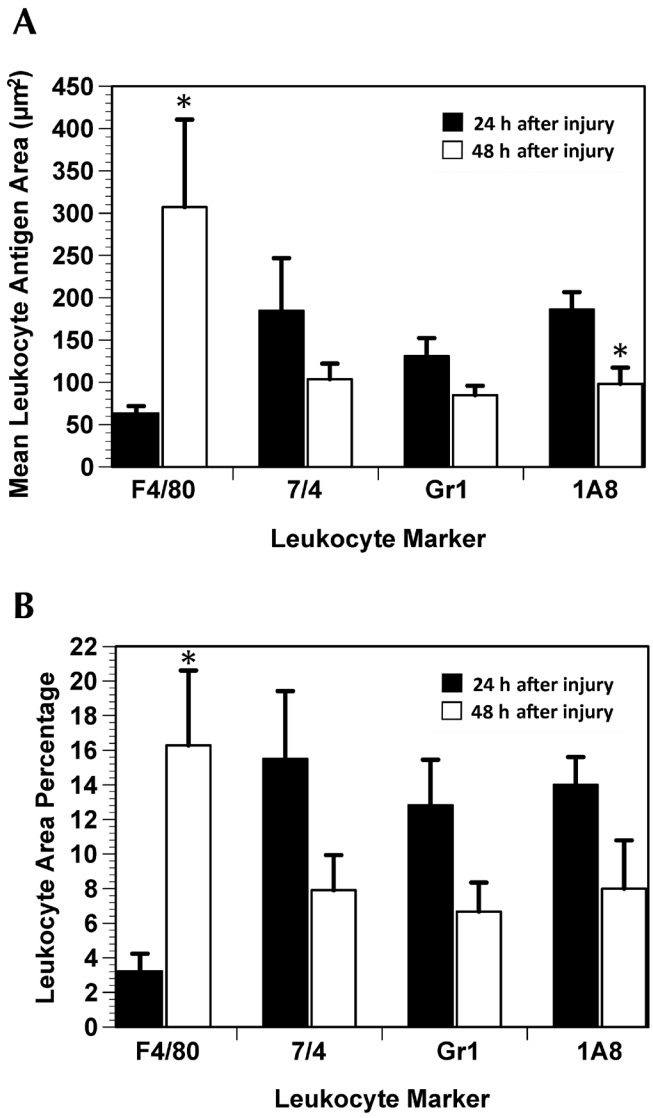

Figure 5. F4/80-, 7/4-, Gr1-, and 1A8-positive leukocyte response to gastrocnemius muscle crush injury (mean ± SE). (A) F4/80-positive macrophages are significantly (*, $P < 0.05$) larger at 48 h compared with 24 h after injury. However, 1A8-positive neutrophils are significantly (*, $P < 0.05$) smaller at 48 h. (B) There is a significant (*, $P < 0.05$) increase in the F4/80 area percentage between the 24- and 48-h time points.

but there was no difference in 7/4 area percentage, number of 7/4-positive cells, mean 7/4 antigen area, Gr1 area percentage, number of Gr1-positive cells, mean Gr1 antigen area, 1A8 area percentage, or number of 1A8-positive cells from 24 to 48 h after injury.

Discussion

According to the current data, we have developed and validated a noninvasive crush injury model for mouse skeletal muscle. In addition to gross assessment of the injuries, muscle damage was verified microscopically and by using leukocyte immunolabeling. To our knowledge, this analysis is the first use of immunolabeling to characterize the specific leukocytes associated with a skeletal muscle crush injury model.

In injured muscle, we observed necrotic fibers with leukocyte infiltration by using hematoxylin and eosin and by immunolabeling for neutrophils (1A8, 7/4, and Gr1 antibodies) and macrophages (CD68 and F4/80 antibodies). Neutrophils and macrophages rapidly invade damaged tissue and contribute to the repair process as sources of growth factors and cytokines and by removing debris.[19] Mean 1A8 antigen area decreased from 24 to 48 h after injury; this finding was expected because neutrophils are the first responders to tissue damage, and their numbers decrease as tissue healing occurs.[20] Macrophages follow the neutrophilic invasion and play a major role in tissue growth and repair.[20] The area percentages and mean antigen areas for the macrophage markers CD68 and F4/80 increased from 24 to 48 h after injury, indicating that activated macrophages were infiltrating the damaged tissue and continuing the process of debridement.[11] These findings indicate that the closed crush injury model is appropriate for the investigation of the pathophysiology of muscle damage and repair.

In addition, our model is a refinement of previous rodent trauma models by reducing the incidence of fibular fractures (10% in our study compared with 27% by using a dropped weight model).[3] The decreased incidence of bone fracture can be attributed to the smaller force applied to the pelvic limb in our study (30 N) compared with previous studies (246 N).[3] We were able to lower the force applied but still obtain measurable muscle damage by ensuring that the piston of the crush injury device was situated firmly against the leg of the mouse; this practice reduced the force of impact that results during the dropped-weight method.

A limitation to our current model is that the investigator is unable to visualize the muscle when applying the crush injury; this drawback may be prohibitive when the injury must be created at a specific site in the muscle. However, even with this limitation, our results indicate that our model is a reproducible method for muscle crush injury in the mouse pelvic limb. Furthermore, our model is a refinement of previous small animal muscle crush injury models, in that it has a lower incidence of bone fracture and reduces animal numbers by eliminating the need for a surgical control group.

Acknowledgments

We thank Sheniz Moonie for her assistance with the statistical analysis. We also thank Kirsten Speck and Jeffrey Kurrus for their assistance with editing this manuscript, and Michael Shappie and David Lee for their assistance in designing the crush injury device.

This material is based on research sponsored by the Air Force Surgeon General's Office under agreement number FA7014-10-2-0001 (awarded to BS). The views and conclusions contained herein are those of the authors and should not be interpreted as necessarily representing the official policies or endorsement, either expressed or implied, of the Air Force Surgeon General's Office or the US Government.

References

1. **Barnard W, Bower J, Brown MA, Murphy M, Austin L.** 1994. Leukemia inhibitory factor (LIF) infusion stimulates skeletal muscle regeneration after injury: injured muscle expresses *lif* mRNA. J Neurol Sci **123:**108–113.
2. **Collins RA, Grounds MD.** 2001. The role of tumor necrosis factor α (TNFα) in skeletal muscle regeneration: studies in TNFα$^{-/-}$ and TNFα$^{-/-}$LTα$^{-/-}$ mice. J Histochem Cytochem **49:**989–1001.
3. **Crisco JJ, Jokl P, Heinen GT, Connell MD, Panjabi MM.** 1994. A muscle contusion injury model: biomechanics, physiology, and histology. Am J Sports Med **22:**702–710.
4. **da Silva R, Gordon S.** 1999. Phagocytosis stimulates alternative glycosylation of macrosialin (mouse CD68), a macrophage-specific endosomal protein. Biochem J **338:**687–694.
5. **Filippin LI, Cuevas MJ, Lima E, Marroni NP, Gonzalez-Gallego J, Xavier RM.** 2011. Nitric oxide regulates the repair of injured skeletal muscle. Nitric Oxide **24:**43–49.
6. **Fleming TJ, Fleming ML, Malek TR.** 1993. Selective expression of Ly6G on myeloid lineage cells in mouse bone marrow: RB6-8C5 mAb to granulocyte-differentiation antigen (Gr1) detects members of the Ly6 family. J Immunol **151:**2399–2408.
7. **Institute for Laboratory Animal Research.** 2011. Guide for the care and use of laboratory animals, 8th ed. Washington (DC): National Academies Press.
8. **Kerkweg U, Schmitz D, de Groot H.** 2006. Screening for the formation of reactive oxygen species and of NO in muscle tissue and remote organs upon mechanical trauma to the mouse hindlimb. Eur Surg Res **38:**83–89.
9. **Kurek JB, Nouri S, Kannourakis G, Murphy M, Austin L.** 1996. Leukemia inhibitory factor and interleukin 6 are produced by diseased and regenerating skeletal muscle. Muscle Nerve **19:**1291–1301.
10. **Malorny U, Michels E, Sorg C.** 1986. A monoclonal antibody against an antigen present on mouse macrophages and absent from monocytes. Cell Tissue Res **243:**421–428.
11. **Mayhew TM, Williams MA.** 1973. The mass and size of normal and activated macrophages—studies with a scanning interferometer. Experientia **29:**80–81.
12. **McBrier NM, Neuberger T, Denegar CR, Sharkey NA, Webb AG.** 2009. Magnetic resonance imaging of acute injury in rats and the effects of buprenorphine on limb volume. J Am Assoc Lab Anim Sci **48:**147–151.
13. **Michaelson M.** 2008. Crush injury, crush syndrome, p 526–531. In: Shapira SC, Hammond JS, Cole LA, editors. Essentials of terror medicine. New Brunswick (Canada): SpringerLink.
14. **Reis ND, Better OS.** 2005. Mechanical muscle-crush injury and acute muscle-crush compartment syndrome. J Bone Joint Surg Br **87:**450–453.
15. **Rosas M, Thomas B, Stacey M, Gordon S, Taylor PR.** 2010. The myeloid 7/4 antigen defines recently generated inflammatory macrophages and is synonymous with Ly6B. J Leukoc Biol **88:**169–180.
16. **Speck K, St. Pierre Schneider B, Deashinta N.** 2011. A rodent model to advance the field treatment of crush muscle injury during earthquakes and other natural disasters. Biol Res Nurs 15**:**17–25.
17. **Stratos I, Graff J, Rotter R, Mittlmeier T, Vollmar B.** 2010. Open blunt crush injury of different severity determines nature and extent of local tissue regeneration and repair. J Orthop Res **28:**950–957.
18. **Takagi R, Fujita N, Arakawa T, Kawada S, Ishii N, Miki A.** 2011. Influence of icing on muscle regeneration after crush injury to skeletal muscles in rats. J Appl Physiol **110:**382–388.
19. **Tidball JG.** 2005. Inflammatory processes in muscle injury and repair. Am J Physiol Regul Integr Comp Physiol **288:**R345–R353.
20. **Tidball JG, Villalta SA.** 2010. Regulatory interactions between muscle and the immune system during muscle regeneration. Am J Physiol Regul Integr Comp Physiol **298:**R1173–R1187.
21. **Winkler T, von Roth P, Matziolis G, Schumann MR, Hahn S, Strube P, Stoltenburg-Didinger G, Perka C, Duda GN, Tohtz SV.** 2011. Time course of skeletal muscle regeneration after severe trauma. Acta Orthop **82:**102–111.
22. **Zouris JM, Walker GJ, Dye J, Galarneau M.** 2006. Wounding patterns for US marines and sailors during operation Iraqi freedom, major combat phase. Mil Med **171:**246–252.